Check for updates

Wideband and continuously-tunable fractional photonic Hilbert transformer based on a single high-birefringence planar Bragg grating

ZIJING ZHANG,[1] CHAOTAN SIMA,[1,2,*] BOLAN LIU,[1] BINCHEN CAI,[1] YUAN GAO,[1] MINMING ZHANG,[1] LI SHEN,[2] YU YU,[2] MENG HUANG,[2] ZHENGGANG LIAN,[3] MATTHEW T. POSNER,[4] JAMES C. GATES,[4] PETER G.R. SMITH,[4] AND DEMING LIU[1]

[1]*Next Generation Internet Access National Engineering Laboratory, School of Optical and Electronic Information, Huazhong University of Science and Technology, Wuhan, 430074, China*
[2]*Wuhan National Laboratory for Optoelectronics, Huazhong University of Science and Technology, Wuhan, 430074, China*
[3]*Yangtze Optical Electronics Co., Ltd. (YOEC), East Lake Hi-Tech Develop zone, Wuhan, 430205, China*
[4]*Optoelectronics Research Centre, University of Southampton, Highfield Campus, SO17 1BJ, Southampton, UK*
*smct@mail.hust.edu.cn

Abstract: We propose and experimentally demonstrate wideband and continuously tunable fractional-order photonic Hilbert transformers (FrHT). These are realized by a single apodized planar Bragg grating within a high-birefringence planar substrate. The fractional order of the FrHT is continuously tuned and precisely controlled by changing the polarization state of the input light. The experimental characterization demonstrates an operating bandwidth up to 120 GHz with amplitude ripples below 3 dB. The optical phase shift response is directly measured to verify the proposed tuning property, demonstrating transform orders of around 1, 0.7, and 0.5. This approach is simple, stable, and compact compared to other existing methods and has great potential in the fields of ultrafast all-optical signal processing.

References and links

1. S. L. Hahn, *Transforms and Applications Handbook* (Chemical Rubber Company, 2010), Chap. 7.
2. C. C. Tseng and S. C. Pei, "Design and application of discrete-time fractional Hilbert transformer," IEEE Trans. Circ. Syst. II. **47**(12), 1529–1533 (2000).
3. A. W. Lohmann, D. Mendlovic, and Z. Zalevsky, "Fractional Hilbert transform," Opt. Lett. **21**(4), 281–283 (1996).
4. C. Cuadrado-Laborde, "Proposal and design of a photonic in-fiber fractional Hilbert transformer," IEEE Photonics Technol. Lett. **22**(1), 33–35 (2010).
5. M. Li and J. Yao, "All-fiber temporal photonic fractional Hilbert transformer based on a directly designed fiber Bragg grating," Opt. Lett. **35**(2), 223–225 (2010).
6. L. Zhuang, M. R. Khan, W. Beeker, A. Leinse, R. Heideman, and C. Roeloffzen, "Novel microwave photonic fractional Hilbert transformer using a ring resonator-based optical all-pass filter," Opt. Express **20**(24), 26499–26510 (2012).
7. M. Burla, M. Li, L. Romero Cortes, X. Wang, L. Chrostowski, and J. Azana, "2.5 THz bandwidth on-chip photonic fractional Hilbert transformer based on a phase-shifted waveguide Bragg grating," in *Proceedings of IEEE Photonics Conference* (IPC IEEE, 2013), pp. 436–437.
8. J. Dong, A. Zheng, Y. Zhang, J. Xia, S. Tan, T. Yang, and X. Zhang, "Photonic Hilbert Transformer Employing On-Chip Photonic Crystal Nanocavity," J. Lightwave Technol. **32**(20), 3704–3709 (2014).
9. H. Shahoei and J. Yao, "Continuously Tunable Fractional Hilbert Transformer by Using a Single pi-Phase Shifted FBG," IEEE Photonics Technol. Lett. **25**(25), 2225–2228 (2013).

10. H. Shahoei, P. Dumais, and J. Yao, "Continuously tunable photonic fractional Hilbert transformer using a high-contrast germanium-doped silica-on-silicon microring resonator," Opt. Lett. **39**(9), 2778–2781 (2014).
11. W. Liu, M. Li, R. S. Guzzon, E. J. Norberg, J. S. Parker, M. Lu, L. A. Coldren, and J. Yao, "A fully reconfigurable photonic integrated signal processor," Nat. Photonics **10**(3), 190–196 (2016).
12. M. T. Posner, R. H. S. Bannerman, D. H. Smith, P. L. Mennea, J. C. Gates, and P. G. R. Smith, "High-birefringence direct-UV-written silica waveguides for heralded single-photon sources at telecom wavelengths," in *2017 European Conference on Lasers and Electro-Optics and European Quantum Electronics Conference*, OSA Technical Digest (online) (2017), paper CM_P_6.
13. S. Sakaguchi, "Consolidation of silica glass soot body prepared by flame hydrolysis reaction," J. Non-Cryst. Solids **171**(3), 249–258 (1994).
14. M. Huang, "Thermal stresses in optical waveguides," Opt. Lett. **28**(23), 2327–2329 (2003).
15. J. B. Spring, P. L. Mennea, B. J. Metcalf, P. C. Humphreys, J. C. Gates, H. L. Rogers, C. Söller, B. J. Smith, W. S. Kolthammer, P. G. R. Smith, and I. A. Walmsley, "Chip-based array of near-identical, pure, heralded single-photon sources," Optica **4**(1), 90–96 (2017).
16. C. Sima, J. C. Gates, H. L. Rogers, P. L. Mennea, C. Holmes, M. N. Zervas, and P. G. R. Smith, "Ultra-wide detuning planar Bragg grating fabrication technique based on direct UV grating writing with electro-optic phase modulation," Opt. Express **21**(13), 15747–15754 (2013).

1. Introduction

Integrated microelectronic circuits have penetrated into every aspect of the field of signal processing, particularly in optical fiber telecommunication systems. Nevertheless, there is increasing exploration of all-optical signal processing due to the unprecedented large bandwidth and fast operating speed. One route uses integrated optical chips to realize photonic Hilbert transforms (PHTs) or Fractional Hilbert Transforms (FrHTs) [1] that can be applied to single sideband modulation or the image edge filtering [2]. The fractional order of Hilbert transformers have provided additonal functionality as they offer control over the phase of a signal, and the signal can be interpreted or encoded [2,3]. These are of particular importance in the field of microwave photonics where processing bandwidths above tens of GHz are extremely challenging.

There have been various endeavours to realize FrHT systems, these include Fiber Bragg Gratings (FBGs) [4,5], silicon-nitride ring resonators [6], phase-shifted gratings in silicon waveguides [7] and photonic crystal nano-cavities [8]. Several tunable FrHT structures have also been reported, including FBG-based interferometric fiber systems [9], micro-ring resonators (MRR) [10] and the InP-InGaAsP integrated ring structure [11]. The fiber-based interferometric systems in [9] allow around 75 GHz (0.6 nm) tunable FrHT operation but require additional separation of the two polarizations hence suffering complexity and poor stability. Likewise, the MRR devices in [10] allow approximately 25 GHz (0.2 nm) tunable FrHT but require tight fabrication accuracy and delicate control of the MMR. The reconfigurable ring structure devices in InP-InGaAsP substrates [11] provide excellent and multifunctional optical processing, including integrator, fractional differentiator as well as around 50 GHz (0.4nm) bandwidth FrHT, but confront considerable fabrication challenges as well as relatively high cost.

In this paper, a simple, wideband and direct route to realize continuously tunable FrHT is proposed and demonstrated with a germano-borosilicate planar substrate. Compared with other existing FrHT devices and systems, this device has benefits of operating bandwidth over 100 GHz, the widest to our knowledge, ultrafast processing capability, a simple compact configuration as well as low cost. A novel structure merely including a polarization rotator and a single silica-on-silicon Bragg grating is employed to realize the continuously tunable FrHT. The high-birefringence (Hi-Bi) chip is obtained with 5×10^{-4} birefringence. By simply changing the incident polarization angle, the ratio of transformed TE-mode signal and non-transformed orthogonal TM-mode signal is precisely controlled, constructing and giving the tunable fractional order processing. Furthermore, the TE/TM mode phase matching condition along the waveguide channel is investigated, to avoid the magnitude degradation and cancelation. In the experiments, a large 120 GHz bandwidth and ≤3 dB ripple amplitude responses are achieved and π, 0.7π, and 0.5π phase shift responses in the frequency domain

are directly measured. The temporal impulse intensity waveforms are also analyzed with measured data. This kind of FrHT devices has strong potential in applications of secure communication systems.

2. Theory analysis

2.1 Operation principle

The original definition of HT is given by the convolution of input signal x(t) and $1/\pi t$

$$H[x(t)] = x(t) * \frac{1}{\pi t} \propto \int_{-\infty}^{\infty} \frac{x(\tau)}{t - \tau} d\tau, \qquad (1)$$

where $H[x(t)]$ is the output of the input x(t) after an ideal conventional Hilbert transform. The Fourier transform of the kernel of conventional HT is given by

$$H(\omega) = -jsgn(\omega), \qquad (2)$$

where ω is the angular frequency and sgn(ω) is the sign function. It is acknowledged that the fractional HT, i.e. FrHT, is a weighed sum of the conventional HT signal and the original signal [1,2], given by

$$H_{Fr}(\omega) = \cos(\varphi) + \sin(\varphi) H(\omega), \qquad (3)$$

where $\varphi = \rho * \pi/2$ and ρ is defined as the fractional order of FrHT. When ρ is equal to 1, the FrHT becomes exactly the conventional HT. The theoretical responses of HT and FrHT in the frequency domain are presented in Fig. 1.
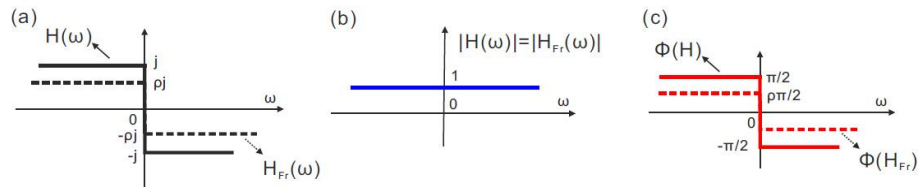

Fig. 1. (a) Theoretical complex responses of HT (solid) and FrHT (dashed); (b) amplitude and (c) phase responses of HT (solid) and FrHT (dashed).

2.2 Device concept

By definition, the Hi-Bi integrated waveguide has intrinsic birefringence such that an integrated Bragg grating has two distinct responses for the TE/TM modes which enables the tuning of the order of the PHT in a compact waveguide structure. The proportions of TE and TM mode light can be controlled by rotating the polarizing maintaining (PM) launch fiber. Due to the birefringent effect of the planar waveguide material, the TE mode spectral response, given by the apodized Bragg grating, is shifted compared with that of the TM mode. By choosing the specific operating zone in the spectrum, only the TE mode (or TM mode) goes through the Hilbert transformation, while the other ratio of orthogonal mode stays non-transformed. Hence, by manipulating the launched polarization state the fractional order of the PHT signal can be tuned. The use of a polarizer in this device clearly requires a fixed polarization input, therefore polarization fluctuations would lead to intensity noise. The schematic diagram of the proposed device and the fractional HT process is demonstrated in Fig. 2.
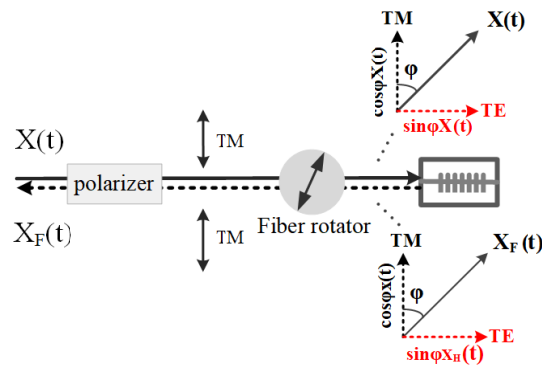
Fig. 2. Schematic diagram of the proposed device and fractional order tuning concept.

Using the Bragg grating transfer matrix method, the amplitude and phase response in frequency domain are numerically analyzed using a Matlab program. The Bragg grating apodization profile is presented in Fig. 3(a). The amplitude responses of TE and TM mode are simulated and are shown in Fig. 3(b) using the grating parameters including a length 12 mm, a grating bandwidth $\Delta f = 250$ GHz, a refractive index modulation depth $\Delta n_{max} = 6 \times 10^{-4}$ and birefringence of 5×10^{-4}.
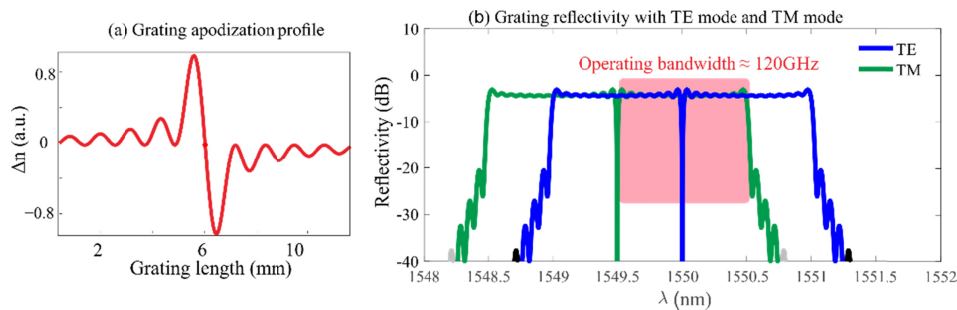

Fig. 3. (a) The PHT grating apodization profile. (b) Grating reflectivity simulation with TE mode (blue) and TM mode (green). The red region shows the designed FrHT operating bandwidth of 120 GHz (1549.5 nm to 1550.5 nm) with the central wavelength of 1550 nm.

As shown in Fig. 3(b), the TE mode (blue line) has the central wavelength of 1550 nm while the TM mode (green line) has a relatively shorter central wavelength of 1549.5 nm. If the optical carrier signal is located at 1550 nm, within the operating bandwidth range between 1549.5 nm and 1550.5 nm (120 GHz) in the red color region, only the TE mode part responds to the conventional (1st order) PHT, while the orthogonal TM part remains unchanged (mirror reflection). The weighted sum of the TE and TM mode light could then construct and provide the fractional order PHT, i.e. FrHT. The fractional order is controlled by adjusting the input light polarization state and the portion between the TE mode and TM mode. The bandwidth of the device is principally defined by the birefringence of the waveguide. The PHT is then designed to utilize the spectral separation afforded by the birefringence, in this case 120 GHz. This bandwidth is limited by the fabrication device parameters, primarily the birefringence of the waveguide and the Bragg grating refractive index contrast.

2.3 Phase matching for polarization mode disperision

The polarization mode disperision of the waveguide yields a spectrally shifted FrHT response between the two polarization modes of the device, thus phase matching of the orthogonal polarization states is investigated in the device. In the previous fiber links [9], it was directly achieved by using the polarization controller. The phase matching condition is calculated as

$$\Delta\phi = \Delta kL = \frac{2\pi\Delta n_{eff}L}{\lambda} = m2\pi ,$$ (4)

where Δn_{eff} is the effective refractive index difference between TE mode and TM mode, also defined as birefringence, L is the extra waveguide for phase matching, λ is the optical carrier wavelength, e.g. 1550 nm in this work, and m is an integer number.
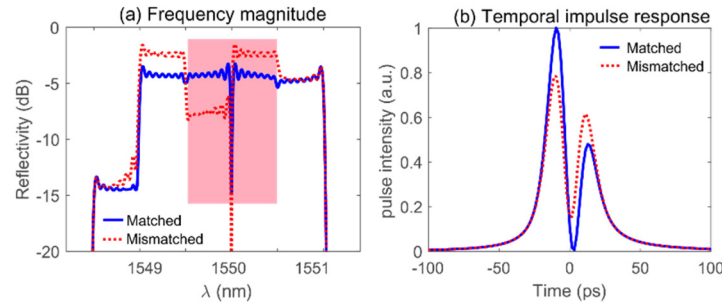

Fig. 4. Comparison between phase-matched (blue solid lines) and phase-mismatched (red dashed lines) scenarios: (a) the frequency amplitude and (b) temporal impulse response of a 0.7 order FrHT. The red region shows the available bandwidth for tunable FrHT operation.

The phase matching effect in frequency amplitude and temporal impulse response for a 0.7 order FrHT is investigated and shown in Fig. 4, with phase-matched scenario (blue solid line) and phase-mismatched scenario (red dashed line). This device has a finite operation bandwidth, as shown in the red region in Fig. 4(a) and its degraded temporal impulse response is illustrated in Fig. 4(b). To achieve the phase-matching condition, the phase compensation is obtained by deliberate design of the propagation length along the waveguide. We have fabricated 16 identical waveguides with different extra propagation lengths, L, and observed the preeminent phase matching condition in the fifth waveguide in the experiment. The experimental tests afterwards have taken into consideration of phase-matching issue.

3. Device fabrication and characterization

After theoretical analysis and simulation, a series of experiments were conducted to realize and verify the tunable FrHT properties.

To obtain a wide operation bandwidth, a large separation of TE and TM mode is required. For this work a Hi-Bi silica-on-silicon platform was developed. The commercial-grade process, flame hydrolysis deposition (FHD), is used to fabricate the silica glass layers. This process has traditionally been used to produce Arrayed Waveguide Gratings (AWGs) and as such has comparable mechanical and thermal stability. These are comprised of a photosensitive core and index-matched over-cladding layers deposited on a thermally oxidized silicon wafer. Meanwhile, photosensitivity and high-birefringence is achieved by controlling the doping process of germanium and boron, while the hydrogen loading is used to further increase the photosensitivity [12].

Both orthogonal polarization mode (TE and TM) are utilized in this work. The reduced germanium and boron dopants of the planar core layer, with respect to the over- and under-cladding, causes a mismatch in the layers' thermal-expansion properties [13]. The mismatch causes stress in the layers and results in an intrinsic birefringence [14]. The dopants, and hence the birefringence, can be precisely controlled by the precursor flow rates, similar to that used in optical fiber fabrication. Our prior work has demonstrated that the birefringence uniformity of our layers is < 1 x 10^{-6} [15]. The resulting tension between the layers also leads to chip bow. In the experiment, around 10 μm of vertical variation was observed when using the 40 mm long chips. This bow can cause misalignment during direct UV grating writing (DGW) [16] and can consequently produce weak gratings. In this work we avoid this problem

by using a small area (2 mm range) within a 20 mm long chip. For longer devices compensation of this chip bend could be achieved by additional vertical translation of the sample during the UV writing process.

The key fabrication technique, the direct UV grating writing (DGW), is a technique that can define both the waveguides and Bragg gratings simultaneously based on the UV photosensitivity of the hydrogen-loaded FHD samples and guarantee the uniform effective refractive index during the process. More detailed information of the DGW technique can be found in the literature [16]. This DGW implementation in the Hi-Bi has also been reported to realize integrated heralded single-photon sources [12,15].

4. Results and discussion

4.1 Characterization setup

Characterization of the tunable FrHT has been demonstrated experimentally. An amplified spontaneous emission (ASE) light source operating in the telecommunications C-band (1530-1570 nm) is used to monitor the device reflection spectral response, as shown in the Fig. 5. After passing through the 3 dB coupler and the polarizer, the input light is polarized and propagates through the polarization maintaining fiber (PMF) into the Hi-Bi PHT grating while the other port of the coupler is terminated. The reflected light propagates back into the optical spectrum analyzer (OSA, AQ6317B) for spectral magnitude analysis. Meanwhile, by using an optical vector network analyzer (OVA 5000, Luna) connected with the fiber polarizer, the grating amplitude, group delay and phase shift is completely characterized in a single wavelength scan. The interrogation of fractional orders is done with a calibrated fiber rotator (HFR007, Thorlabs), which was obtained by detecting TE mode intensity when changing the polarization angle. The calibration data showed in the inset of Fig. 5 indicate that it is possible to continuously and periodically tune the angle of launch of the polarization in this experimental setup.
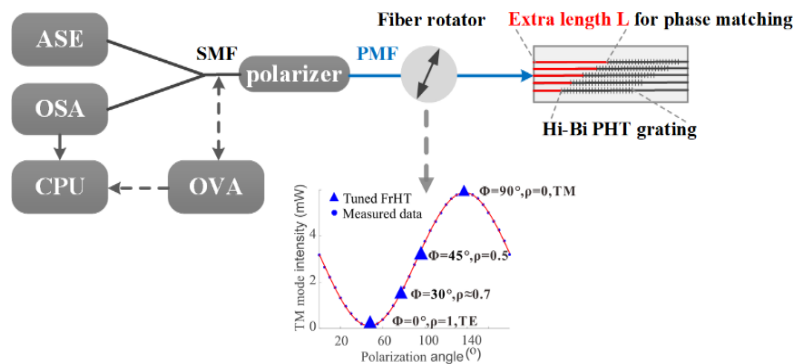

Fig. 5. Experimental setup of the characterization system and the planar chip layout; Inset: calibration curves of the fiber rotator. The triangle points show the rotating angle φ and corresponding fractional order ρ, with 0°, 30°, 45° and 90°. Abbreviations: ASE: amplified spontaneous emission light source. OSA; optical spectrum analyzer. CPU; computer. OVA: optical vector network analyzer. SMF: single mode fiber. PMF: polarization maintaining fiber.

Here, 16 identical Hi-Bi PHT grating waveguides with different extra waveguide lengths, L, (from 1 mm to 2.5 mm, with 100 µm separation between waveguides) are written in a single chip, as schematically shown in Fig. 5. By shifting and coupling to different waveguides across the chip, the optimized waveguide with phase-matching condition could be observed and selected. By using this characterization setup, the measured data are presented and analyzed in the following sections.

4.2 Reflective amplitude response

The amplitude response in the frequency domain was measured and compared with the simulation. The-phase matched waveguide is compared with the phase-mismatched waveguide, to further illustrate the importance of the phase-matching condition.

The reflectivity responses of the waveguides with 12 mm PHT grating in the planar chip are measured with TE mode and TM mode respectively, as shown in Fig. 6(a). For the TE mode, the smooth flat-top amplitude response and broad bandwidth (from 1548.5 nm to 1550.5 nm) around central wavelength 1549.5 nm is principally evident when $\rho = 1$ as the conventional PHT. Hence the FrHT operating bandwidth here is around 120 GHz, the red color region, located from 1549 nm to 1550 nm. Figure 6(a) presents the reflective amplitude responses of TE mode ($\varphi = 0°$, $\rho = 1$, blue solid line) and TM mode ($\varphi = 90°$, $\rho = 0$, green solid line), respectively. The grating simulation (red dotted line) is also exhibited for verification.
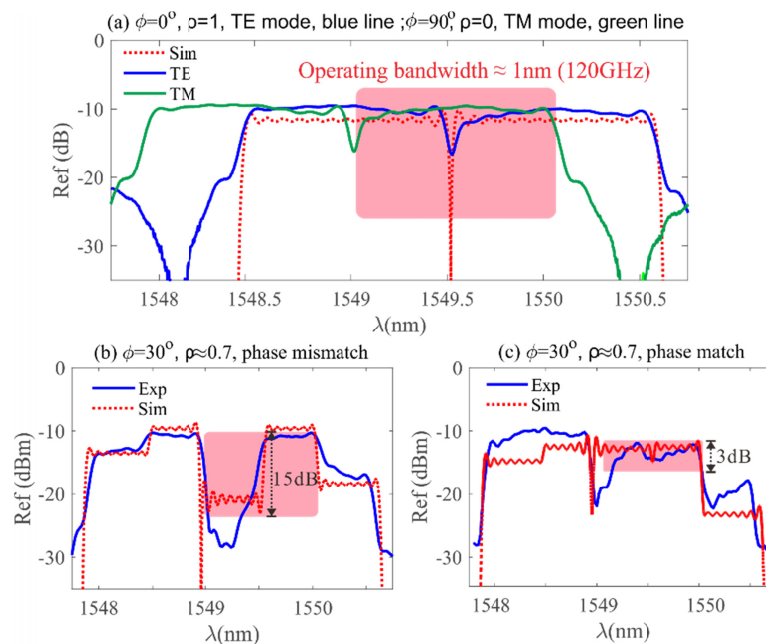

Fig. 6. Simulated and experimental reflectivity of the FrHT waveguides with (a) the rotating angle of 0° and 90°, corresponding to $\rho = 0$ (TE mode) and $\rho = 1$ (TM mode); (b) the rotating angle of 30°, $\rho \approx 0.7$ without phase matching condition; (c) the rotating angle 30°, $\rho \approx 0.7$, with phase matching condition.

Then, when rotating the polarization angle to 30°, that is the fractional order $\rho \approx 0.7$ in principle, the device reflection amplitude is measured. Figure 8(b) shows the fractional order amplitude ($\varphi = 30°$, $\rho \approx 0.7$) in the phase mismatching scenario while Fig. 6(c) is the phase matching scenario, and the simulated data is also plotted (red dotted lines) for comparison. It is obvious that the cancelation of the amplitude (over −15 dB) would occur when TE/TM mode is phase mismatched, unfeasible for FrHT operation. When the phase-matching condition is fulfilled, the amplitude becomes flat-top across the wideband, with less than 3 dB variation. In this case, the device could be utilized as the FrHT and the optical phase response is directly measured by using the OVA.

To be noted, since the extra length L is selected with 100 μm increment in the experiment, the optical phase may not be perfectly matched in the experiments, which would lead to the 3dB degradation and distortion of the amplitude response in Fig. 6(c). Nevertheless, the

experimental results show favorable agreement in shape and trend with the simulated FrHT, and the vital phase jump is measured for further verification.

4.3 Phase shift measurement

The phase response is the most essential feature for the FrHT processing. Principally, there should be a phase jump at the central wavelength, and the value of phase jump is in direct proportion to the fractional order of the transformation. Using the Luna OVA5000, the phase jump at the central wavelength has been directly measured. As Fig. 7 shows, the phase jump at around 1549 nm in the 12 mm grating waveguide is 3.1 rad ($\approx \pi$) for $\rho = 1$, 2.1 rad ($\approx 0.7\pi$) for $\rho = 0.7$, and 1.6 rad ($\approx 0.5\pi$) for $\rho = 0.5$, respectively. The linear relationship between the fractional order ρ and phase jump is plotted in Fig. 7(d). All phase data are compensated linearly for illustrative purposes. Compared with the ideal phase response in Fig. 1(c), the measured phase responses in Fig. 7 behave as the temporal delay, the expected tendency due to causality.
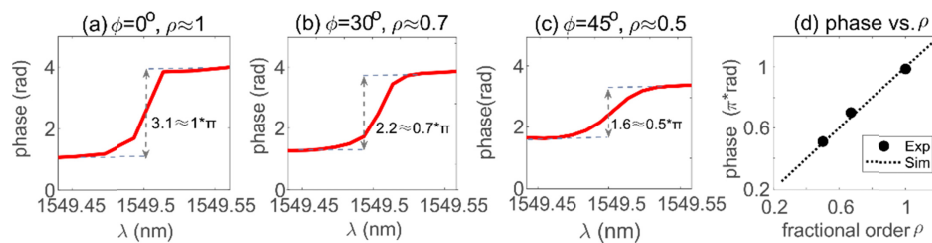

Fig. 7. Measured phase responses with tunable fractional order (a) $\rho = 1$ with phase jump of π; (b) $\rho = 0.7$ with phase jump of 0.7π; (c) $\rho = 0.5$ with phase jump of 0.5π; (d) Relationship between phase jump and fractional order ρ with simulation and experiment results.

There are still some sidebands and ripple noises in the amplitude responses in Fig. 6 and the manipulation of fractional orders is not perfect as shown in Fig. 7. Firstly, the HT grating, shown in (a), includes a π phase shift requiring a grating period translation of half a period (~270 nm). The DGW technique has an intrinsic 10 nm positional error. Hence, there could result in around 3.7% error in phase shift. Secondly, the fiber rotator (HFR007, Thorlabs) used in the experiments has the engraved dial with 5-degree increment graduations, which may also cause about 2.8% error. This could be improved with an upgraded fiber rotator or an automated polarization controller.

4.4 Temporal intensity analysis

To investigate the impact of the fabrication imperfections evident in the spectral response, the temporal response of the FrHT is calculated, and compared with the ideal transformation. Here we use the experimentally measured reflectivity amplitude and phase response in the frequency domain to construct the FrHT filter response in the temporal domain. Figure 8 shows a simulation of the temporal transformation of a Gaussian pulse, with 25 GHz Full Width at Half Maximum (FWHM) with a carrier wavelength of 1549.5 nm. Figures 8(a) and 8(b) show the fractional orders of $\rho \approx 0.7$ and $\rho \approx 0.5$ respectively. The input temporal signal is shown by the black dotted lines and the calculated output pulse waveform of our device is show by the blue solid lines. This response can be compared with the simulated waveform from an ideal FrHT, shown by the red solid lines. It is observed that the temporal impulse waveforms of our FrHT and the ideal FrHT show favorable consistency, with a calculated root mean square error of 1.8% and 2.6% for the fractional orders of $\rho \approx 0.7$ and $\rho \approx 0.5$ respectively.
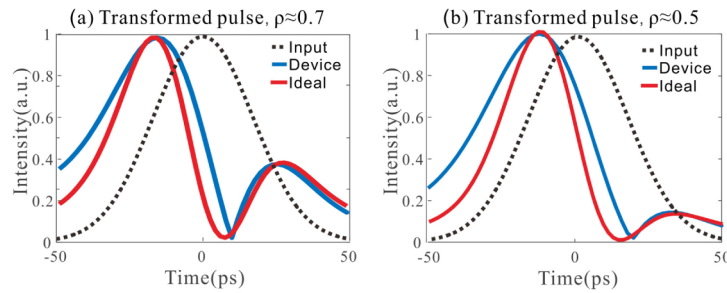
Fig. 8. Calculated transformed pulse waveform of (a) ρ≈0.7 FrHT (b) ρ≈0.5 FrHT. Input Gaussian pulse (black dotted lines); Calculated FrHT output pulses of the presented device (blue solid lines); Ideal FrHT output pulses (red solid lines).

5. Conclusion

In conclusion, a 120 GHz wide bandwidth and continuously tunable integrated fractional order photonic Hilbert transformer is proposed and experimentally demonstrated, offering stability and simplicity, as well as relatively low cost compared with other existing methods. By changing the incident angle of polarization to control the TM transformed portion and TE non-transformed portion, the tunable order FrHT is achieved. A birefringence of 5×10^{-4} silica-on-silicon planar substrate was developed. The Hi-Bi sample deposition, grating fabrication and device characterization are thoroughly presented. The 1, 0.7 and 0.5 order FrHT has been successfully realized and tested. The experimental results with amplitude and phase responses infrequency domain and temporal intensity responses are completely analyzed and agree soundly with the ideal simulation. By investigating higher birefringence waveguides, it will be possible to make devices with even wider operating bandwidths for use as microwave photonic filters. This integrated tunable FrHT is promising for future implementations in ultrafast all-optical signal processing.

Funding